The Canadian Mineralogist
Vol. 40, pp. 519-526 (2002)

THE SYSTEM Fe–Rh–S AT 900° AND 500°C

EMIL MAKOVICKY[§], MILOTA MAKOVICKY AND JOHN ROSE-HANSEN

Geological Institute, University of Copenhagen, Øster Voldgade 10, DK-1350 Copenhagen K, Denmark

ABSTRACT

The condensed phase system Fe–Rh–S was studied by means of dry syntheses at 900° and 500°C. At 900°C, there are fields of γ(Fe,Rh) with up to 29.7 at.% Rh, α_1(Fe,Rh) with 40–50.4 at.% Rh and γ(Rh,Fe) between 0 and 34.3 at.% Fe, $Fe_{1-x}S$ that dissolves up to 25.7 at.% Rh at 55 at.% S, sulfide melt centered on ~37.5 at.% S and 40 at.% Rh, $Rh_{17}S_{15}$ (up to 7.5 at.% Fe), Rh_3S_4, Rh_2S_3 and $Rh_{2.75}S_{7.25}$ ("RhS_3") dissolving up to 4 at.% Fe. At 500°C, α(Fe,Rh) contains up to 9.5 at.% Rh, α_1(Fe,Rh) has 33.5–52.2 at.% Rh, followed by γ(Rh,Fe). $Fe_{1-x}S$ dissolves up to 2.8 at.% Rh at 52.5 at.% S. Thiospinel $Fe(Fe_{0.08}Rh_{1.92})S_4$ is associated with FeS_2, $Rh_{17}S_{15}$ (up to 4 at.% Fe) and Rh_2S_3. "RhS_3" contains less than 1 at.% Fe. The principal assemblages are defined for both temperatures. We discuss data from the partly studied Fe–Ni–Rh–S system and compare the partition patterns of Rh inferred from the current study with those from sulfide–PGE deposits.

Keywords: Fe–Rh–S system, Fe–Rh alloys, Rh sulfides, pyrrhotite, phase equilibria.

SOMMAIRE

Nous avons étudié le système à phases condensées Fe–Rh–S par synthèses à sec à 900° et à 500°C. A 900°C, nous documentons des champs de stabilité de γ(Fe,Rh) contenant jusqu'à 29.7% Rh (proportion d'atomes), α_1(Fe,Rh) avec entre 40 et 50.4% de Rh et γ(Rh,Fe) contenant entre 0 et 34.3% de Fe, $Fe_{1-x}S$ qui dissout jusqu'à 25.7% de Rh à 55% de S, un liquide sulfuré centré sur ~37.5% S et 40% Rh, $Rh_{17}S_{15}$ (jusqu'à 7.5% de Fe), Rh_3S_4, Rh_2S_3 et $Rh_{2.75}S_{7.25}$ ("RhS_3") qui dissout jusqu'à 4% de Fe. A 500°C, la phase α(Fe,Rh) contient jusqu'à 9.5% de Rh, α_1(Fe,Rh) contient entre 33.5 et 52.2% de Rh, suivi par γ(Rh,Fe). Le sulfure $Fe_{1-x}S$ dissout jusqu'à 2.8% de Rh à 52.5% de S. Le thiospinelle $Fe(Fe_{0.08}Rh_{1.92})S_4$ est associé à FeS_2, $Rh_{17}S_{15}$ (jusqu'à 4% de Fe) et Rh_2S_3. La phase "RhS_3" contient moins de 1% de Fe. Nous définissons les assemblages principaux aux deux températures. Nous fondons notre discussion sur les résultats apportés du système Fe–Ni–Rh–S, partiellement étudié, et nous comparons la répartition du Rh préconisée à partir des résultats d'expériences avec celle dans les gisements de sulfures contenant les éléments du groupe du platine.

(Traduit par la Rédaction)

Mots-clés: système Fe–Rh–S, alliages Fe–Rh, sulfures de Rh, pyrrhotite, équilibre de phases.

INTRODUCTION

The present study of the system Fe–Rh–S contributes to the understanding of the distribution of rhodium in PGE (platinum-group elements) deposits rich in Fe at 900°C, *i.e.*, at submagmatic temperatures, and at 500°C, *i.e.*, in postmagmatic and metamorphic processes. It answers some of the questions raised by the recent exploration activity connected with the augmented interest in rhodium in the past few years. Previous investigations of rhodium-containing sulfide systems were made by Distler *et al.* (1977, 1988), who studied the crystallization of Fe–Rh–Ni–S melts and exsolution processes in their products, Bryukvin *et al.* (1990), who investigated high-temperature phase equilibria in the Fe–Rh–S system, Sinyakova *et al.* (1994), who investigated the FeS–Ni_2S_3 system with 1 wt% Rh added, at 817° and 600°C, and during slow cooling, and by Makovicky *et al.* (1986), who presented preliminary data on the system Fe–Rh–S at 900° and 500°C, Rh-rich pentlandite at 500°C, and exploratory studies in the Fe–Rh–Cu–S system at 900° and 500°C. Several investigators (Blase & Schipper 1964, Harada 1973, Tretyakov *et al.* 1977) studied Fe–Rh thiospinels. Massalski *et al.* (1986) summarized previous work on the system Fe–Rh.

In the present study, we completed and refined the preliminary descriptions of the system Fe–Rh–S at 900°

§ *E-mail address*: emilm@geo.geol.ku.dk

and 500°C of Makovicky *et al*. (1986) and Makovicky *et al*. (1992).

Experimental

Fifty-six 150-mg charges were weighed out from pure elements (Johnson Matthey's Specpure rhodium sponge with 40 ppm metal impurities, freshly filed Specpure Fe rods with 20–25 ppm of metal impurities and pure S (>99.999%, Fluka). They were sealed in evacuated silica glass tubes, preheated at 300°C, and annealed at the desired temperatures for periods of up to 30 days. After regrinding and homogenization, they were resealed and annealed for 60–90 days.

The quenched products were studied in polished sections with reflected light microscopy and by means of electron-microprobe analyses. A JEOL Superprobe was used in wavelength-dispersion mode, with an on-line correction program supplied by JEOL. Rh metal and natural $CuFeS_2$ were used as standards. Wavelengths employed were Rh*L*α, Fe*K*α, and S*K*α; acceleration voltage was 20 kV, sample current 30 or 20 nA, and counting times, 20 s. A number of measurements were taken on each phase present, spread over the entire sample. Compositions of solidified melt were studied by sweeping the beam over rectangular areas, the size of which was selected according to the grain size of the quenched aggregate. Principal results are given in Table 1. Detection limits, determined using pure standards without minor elements, are 0.1 wt% Ni, 0.1 wt% Fe and 0.1 wt% Rh.

Phase Relations at 900°C

At 900°C, the condensed system Fe–Rh–S contains a broad range of Fe–Rh alloys, five binary sulfides (three of which reach far into the ternary region), and a small field of sulfide melt near the central part of the system (Fig. 1).

Our results show that the solid-solution fields of Fe–Rh alloys are as follows: γ(Fe,Rh) contains up to 29.7 at.% Rh, α_1(Fe,Rh) contains 40–50.4 at.% Rh, and γ(Rh,Fe) extends between 0 and 34.3 at.% Fe (Fig. 1). The pyrrhotite (*po*) compositions associated with the two-alloy assemblages are $Fe_{\leq 50}Rh_{0.03}S_{\geq 50}$ and $Fe_{44.7}Rh_{4.0}S_{51.3}$, respectively.

The two-phase fields pyrrhotite–alloy and $Rh_{17}S_{15}$–alloy are separated from each other by phase assemblages that involve a liquid field centered on a composition of approximately 37.5 at.% S, 40 at.% Rh and 22.5 at.% Fe, and 5 to 7 at.% broad in different directions. The three-phase assemblages pyrrhotite (7 at.% Rh, 52 at.% S) – alloy (68.5 at.% Rh) – sulfide melt, $Rh_{17}S_{15}$ (>7 at.% Fe) – alloy (70.5 at.% Rh) – melt, and

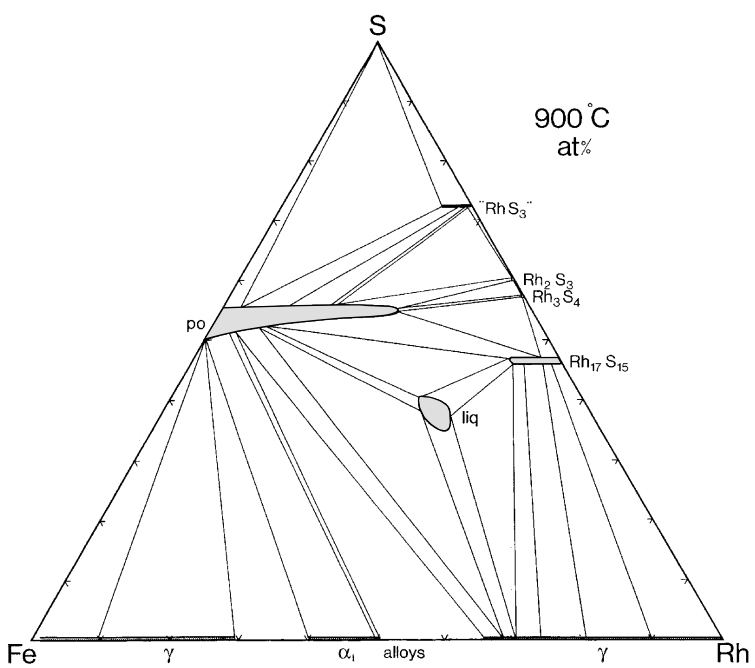

FIG. 1. The system Fe–Rh–S at 900°C. Width of field for solid phases (including alloys) is schematic except for pyrrhotite (*po*) and $Rh_{17}S_{15}$.

TABLE 1. PHASE COMPOSITIONS IN SELECTED CHARGES, SYSTEM Fe–Rh–S AT 900° AND 500°C

T/Charge	Phase	Fe	Rh	S	Total
9H2	po (2)	53.67(9)	6.19(18)	40.65(6)	100.51
	po (4)	53.10(24	6.88(40)	40.69(6)	100.67
9H4	po (7)	55.72(41)	7.45(14)	36.03(27)	99.20
	alloy (3)	35.48(22)	65.23(59)	0.06(1)	100.77
9H7	po (11)	56.17(31)	7.66(11)	35.83(24)	99.66
	alloy (8)	35.70(30)	64.79(33)	0.05(3)	100.54
	alloy (2)	22.63(44)	78.05(96)	0.01(1)	100.69
9H1	po (8)	55.02(13)	9.07(36)	35.85(24)	99.94
	po (3)	55.24(34)	9.07(10)	36.26(53)	100.57
	alloy (9)	22.18	78.30(91)	0.04(4)	100.52
9H11	po (18)	24.06(32)	43.51(45)	33.14(23)	100.71
	(3)	63.20(5)	0.05(5)	35.88(17)	99.13
	po (2)	24.35(40)	44.03(54)	33.14(55)	101.52
9H12	po (16)	29.33(23)	37.60(31)	33.01(13)	99.94
	po (3)	29.35(22)	37.92(42)	33.59(32)	100.86
9H15	po (5)	61.87(10)	0.04(0)	35.91(6)	97.82
	alloy (2)	57.72(22)	41.80(14)	0.03(0)	99.55
9H14	po (4)	64.39(29)	0.09(9)	36.88(34)	101.36
	alloy (4)	85.10(100)	17.01(54)	0.03(1)	102.14
9H16	Rh_2S_3 (6)	0.17(0)	67.53(149)	31.10(150)	98.80
	po (4)	19.95(1)	48.61(16)	31.91(4)	100.47
	po (3)	19.88(4)	46.67(80)	31.90(2)	98.45
9H17	po (3)	31.54(27)	32.31(47)	36.02(38)	99.87
	RhS_3 (2)	1.12(3)	52.33(1)	45.82(1)	99.27
	RhS_3 (2)	1.09(17)	52.53(44)	45.78(12)	99.40
9H18	po (4)	50.95(18)	14.89(13)	35.79(38)	101.63
	liq (4)	14.84(79)	68.93(121)	18.02(29)	101.79
	liq (2)	11.19(12)	73.12(35)	17.52(42)	101.83
9H13	po (2)	41.12(3)	20.54(27)	37.95(6)	99.61
	RhS_3 (5)	1.5(19)	52.71(18)	44.73(17)	98.94
9H22	$Rh_{17}S_{15}$ (4)	2.04(2)	76.72(21)	22.48(13)	101.24
	po (2)	20.28(17)	48.07(20)	32.99(95)	101.34
	$Rh_{17}S_{15}$ (2)	2.01(6)	75.84(183)	22.09(51)	99.94
	$Rh_{17}S_{15}$ (12)	1.99(4)	76.46(48)	22.44(50)	100.89
	po (8)	20.21(13)	47.46(47)	32.46(27)	100.13
9H21	$Rh_{17}S_{15}$ (6)	5.09(7)	72.47(21)	22.17(18)	99.73
	po (5)	47.01(39)	17.13(28)	35.13(24)	99.27
	po (4)	47.07(13)	17.24(10)	34.81(9)	99.12
	liquid (7)	19.41(83)	60.97(185)	19.03(101)	99.41
	alloy (3)	14.55(9)	76.44(12)	0.00(0)	
	$Rh_{17}S_{15}$ (3)	4.83(6)	74.3(13)	21.52(7)	100.65
	$Rh_{17}S_{15}$ (3)	6.21(3)	72.58(44)	21.9(30)	100.69
9H23	RhS_3(5)	0.88(34)	54.00(13)	45.47(21)	100.35
	po (4)	30.38(87)	32.70(86)	35.72(26)	98.80
	Rh_2S_3 (2)	0.36(4)	67.81(15)	32.51(17)	100.18
	RhS_3 (5)	0.88(61)	53.41(12)	45.47(21)	99.76
	po (4)	30.38(87)	32.34(85)	35.72(26)	98.44
	Rh_2S_3 (4)	0.35(5)	66.70(20)	32.66(5)	99.71
9H26	alloy (5)	12.55(37)	87.34(64)	0.01(2)	99.90
	$Rh_{17}S_{15}$ (5)	2.94(17)	76.20(28)	21.70(14)	100.84
	alloy (3)	12.88(52)	86.01(63)	0.07(4)	98.80
	$Rh_{17}S_{15}$ (5)	3.02(6)	75.41(47)	21.25(20)	100.14
	liq (3)	18.45(25)	55.85(26)	19.03(27)	93.33
	alloy (3)	20.60(21)	80.68(9)	0.00(0)	101.28
9H27	alloy (5)	5.45(12)	94.53(29)	0.02(3)	99.98
	$Rh_{17}S_{15}$ (3)	1.12(4)	76.03(52)	21.58(9)	99.79
	$Rh_{17}S_{15}$ (5)	3.02(6)	75.41(47)	21.25(20)	99.68
	alloy (3)	12.88(52)	86.01(63)	0.07(4)	98.96
	$Rh_{17}S_{15}$ (5)	1.13(5)	78.38(53)	21.93(20)	101.44
	alloy (2)	5.15(17)	94.53(39)	0.00	99.68
9H28	alloy (4)	18.59(19)	81.07(21)	0.00(0)	99.66
	coarse (6)	18.73(137)	62.54(229)	17.96(94)	99.23
	fine (4)	17.51(8)	64.83(55)	17.02(59)	99.36
9H29	alloy (2)	19.64(8)	80.07(37)	0.00(0)	99.71
	$Rh_{17}S_{15}$ (3)	5.29(3)	73.65(26)	21.84(52)	100.78
	alloy (2)	19.99(3)	80.81(56)	0.00(0)	100.80
	po (2)	48.43(62)	15.66(13)	35.43(21)	99.52
	melt (5)	18.87(129)	61.18(176)	18.79(30)	98.84
9H30	$Rh_{17}S_{15}$ (4)	2.41(6)	75.97(37)	21.50(19)	99.88
	$Rh_{17}S_{15}$ (4)	2.31(2)	76.47(43)	21.60(26)	100.38
	alloy (5)	10.15(11)	89.93(45)	0.01(2)	100.09
9H31	$Rh_{17}S_{15}$ (5)	4.89(7)	74.22(42)	21.67(22)	100.78
	$Rh_{17}S_{15}$ (7)	4.81(8)	72.42(35)	21.45(34)	98.68
	po (5)	44.33(24)	20.41(20)	34.38(22)	99.12
9H32	po (6)	52.77(46)	6.18(40)	39.92(4)	98.87
9H11-3	(3)	27.49(52)	45.57(62)	28.04(45)	101.10
	(3)	22.77(61)	43.95(43)	33.21(28)	99.93
9R1	po (17)	61.67(37)	0.06(6)	36.52(42)	98.29
	alloy (11)	56.12(34)	43.71(37)	0.05(13)	99.92
9R21	alloy (10)	56.07(42)	43.33(34)	0.11(25)	99.57
	po (4)	61.46(95)	0.06(9)	36.60(24)	98.16
9R21B	po (4)	30.01(151)	33.71(133)	36.57(23)	100.40
	RhS_3 (4)	0.87(7)	54.51(58)	45.90(33)	101.32
	Rh_2S_3 (3)	0.30(2)	68.05(26)	32.29(25)	100.67
9R3	po (3)	31.70(37)	31.32(43)	36.81(13)	99.87
	RhS_3 (3)	1.10(15)	53.40(27)	45.03(63)	99.55
	Rh_2S_3 (2)	0.33(2)	67.36(8)	31.87(21)	99.59
9R2	po (4)	30.73(85)	29.35(102)	35.42(26)	95.56
	RhS_3 (3)	2.21(67)	50.74(54)	43.29(42)	96.27
9R3	RhS_3 (8)	2.77(53)	49.70(55)	46.44(66)	98.98
	RhS_3 (3)	4.19(36)	47.87(42)	46.54(11)	98.67
5R1	po (10)	62.89(40)	0.03(3)	36.11(36)	99.08
	alloy (5)	84.00(175)	16.35(167)	0.02(1)	100.42
	alloy (2)	88.70(14)	11.26(3)	0.11(14)	100.15
5R2	po (15)	62.01(76)	0.06(6)	36.04(100)	98.17
	alloy (3)	46.91(87)	53.72(30)	0.01(1)	100.70
	alloy (2)	42.82(61)	57.60(33)	0.01(0)	100.45
5R3	$Rh_{17}S_{15}$ (6)	3.39(42)	75.24(57)	21.18(38)	99.87
	alloy (3)	0.15(11)	99.41(163)	0.23(39)	99.84
	alloy (3)	2.45(59)	74.77(54)	20.98(18)	98.26
5R4	$Rh_{17}S_{15}$ (6)	3.46(19)	75.82(47)	21.05(28)	100.35
	alloy	0.18(18)	101.30(104)	0.01(1)	101.47
5R4	alloy (2)	0.83(7)	95.82(37)	2.64(50)	99.39
	$Rh_{17}S_{15}$ (5)	3.71(66)	74.25(52)	20.51(22)	98.57
	alloy (2)	0.21(15)	96.79(126)	0.53(74)	97.55
5R5	Rh_2S_3 (12)	0.24(21)	66.66(65)	31.22(45)	98.17
	py (7)	45.01(36)	0.11(13)	52.47(46)	97.66
	Rh_2S_3 (2)	0.26(11)	67.60(20)	31.32(11)	99.21
	Rh_2S_3 (8)	0.29(13)	65.92(55)	31.20(29)	97.47
	py (3)	43.07(11)	0.97(18)	51.51(31)	95.60
	py (3)	44.22(49)	0.11(14)	51.94(75)	96.34
	py (5)	44.80(14)	0.10(14)	51.88(75)	96.86
5R6	Rh_2S_3 (12)	0.31(27)	65.92(57)	30.83(26)	97.10
	py (8)	44.03(42)	0.53(49)	51.83(26)	96.45
	$Rh_{17}S_{15}$ (2)	0.04(2)	76.39(14)	20.73(32)	97.21
	Rh_2S_3 (2)	8.59(45)	54.56(71)	36.53(2)	99.73
	RhS_3 (2)	0.07(0)	54.13(30)	42.23(263)	96.45

TABLE 1 (continued). PHASE COMPOSITIONS IN SELECTED CHARGES, SYSTEM Rh–Fe–S AT 900° AND 500°C

T/Charge	Phase	Fe	Rh	S	Total
5R1	po (5)	59.46(24)	0.10(6)	36.52(26)	96.19
5R2	po (2)	57.46(289)	0.03(3)	35.30(110)	92.83
	po1 (2)	58.75(58)	0.02(1)	36.23(13)	95.07
	alloy (2)	42.32(86)	55.59(5)	0.01(0)	97.94
5R3	rhodium (3)	0.27(15)	100.30(20)	0.01(0)	100.60
	$Rh_{17}S_{15}$ (3)	2.66(77)	74.52(64)	20.97(20)	98.18
5R5	Rh_2S_3 (4)	0.23(13)	67.29(42)	32.05(35)	99.61
	py (4)	43.43(67)	0.04(7)	53.08(140)	97.05
5R6	$Rh_{17}S_{15}$ (2)	0.02(1)	74.33(13)	21.77(62)	96.26
	Rh_2S_3 (3)	0.06(1)	66.40(83)	31.61(45)	98.10
	py (4)	43.57(52)	0.06(8)	53.68(43)	97.36
5H7	rhodium (5)	0.64(16)	99.82(134)	0.05(2)	100.51
	po (3)	62.92(45)	0.73(14)	36.65(27)	100.30
	po (7)	63.51(37)	0.11(7)	36.74(37)	100.36
	alloy (3)	37.21(24)	61.99(163)	0.06(1)	99.26
5H13	rhodium (2)	0.54(7)	101.80(1)	0.06(0)	102.38
	$Rh_{17}S_{15}$ (3)	4.77(28)	75.26(64)	21.53(28)	101.56
	po (2)	61.45(36)	1.13(18)	36.11(33)	98.69
5H11	spinel (6)	15.44(52)	51.12(101)	33.55(9)	100.11
	Rh_2S_3 (3)	0.59(25)	67.15(3)	32.91(2)	100.65
	po (1)	56.94	4.32	36.98	98.24
	po (1)	55.93	5.42	36.82	98.17
	po (1)	57.43	3.54	37.48	98.45
	Rh_2S_3 (3)	0.42(13)	65.96(16)	33.01(7)	99.39
5H10	po (3)	58.08(37)	3.35(27)	37.43(6)	98.86
	po (3)	57.60(24)	4.46(19)	37.25(20)	99.31
	$Rh_{17}S_{15}$ (4)	3.34(34)	74.36(46)	22.63(29)	100.33
	$Rh_{17}S_{15}$ (3)	3.18(34)	74.99(50)	22.65(3)	100.82
5H6	po (7)	62.20(17)	0.07(6)	37.42(28)	99.62
	py (2)	36.94(108)	0	61.42(88)	98.36
	sulfur (2)	0.66(21)	0	97.15(11)	97.81
5H9	$Rh_{17}S_{15}$ (4)	4.1(37)	73.84(18)	22.05(26)	99.99
	~alloy (4)	27.2(163)	65.94(73)	6.23(121)	99.37
	po (4)	61.02(23)	1.17(11)	36.95(48)	99.14
5H8-40	$Rh_{17}S_{15}$ (6)	3.36(18)	74.44(58)	22.78(21)	100.58
	Rh_2S_3 (5)	0.43(21)	67.37(47)	33.47(44)	101.27
	po (7)	56.05(45)	6.35(25)	36.75(25)	99.15
	spinel (2)	15.72(2)	50.89(15)	33.84(8)	100.45
5H8-41	~alloy (6)	26.83(268)	67.93(135)	6.47(180)	101.23
	po (3)	60.99(27)	1.29(19)	36.72(23)	99.00
	po (2)	61.67(14)	0.78(14)	36.82(28)	99.27
	$Rh_{17}S_{15}$ (3)	4.42(29)	75.77(76)	21.94(12)	102.13
5H14	alloy (2)	40.89(20)	59.51(67)	0.06(2)	100.46
	po (2)	62.55(21)	0.13(18)	35.60(17)	98.28
	po (2)	62.75(21)	0.13(18)	35.57(17)	98.45
	rhodium (1)	5.48	96.65	0	102.13
5H3	po (5)	59.58(158)	1.57(162)	37.67(14)	98.82
	po (4)	57.19(17)	4.09(11)	37.56(3)	98.84
	po (3)	58.78(45)	2.61(12)	37.47(14)	98.86
	Rh_2S_3 (2)	0.67(32)	67.22(65)	32.57(8)	100.46
	$Rh_{17}S_{15}$ (2)	3.23(16)	74.14(7)	21.94(3)	99.31
	$Rh_{17}S_{15}$ (2)	3.12(8)	75.29(48)	22.04(19)	100.45
	spinel (2)	15.43(6)	50.93(12)	33.46(12)	99.82
	Rh_2S_3 (2)	0.38(8)	68.42(33)	32.20(24)	101.00
5H1	$Rh_{17}S_{15}$ (4)	4.61(25)	75.02(114)	21.19(14)	100.82
	po (7)	62.13(28)	0.88(15)	37.37(4)	100.38
	$Rh_{17}S_{15}$ (5)	3.72(18)	75.95(60)	21.54(10)	101.21
5H18	$Rh_{17}S_{15}$ (11)	0.05(4)	78.06(89)	21.8(42)	99.91
	~Rh_2S_3 (9)	0.11(5)	68.14(91)	31.88(32)	100.13
5H15	py (2)	46.23(106)	0.12(3)	52.60(24)	98.95
	py (4)	47.76(112)	0.03(5)	52.27(54)	100.06
	po (2)	59.78(7)	0.00(0)	38.10(5)	97.88
	py (2)	48.40(14)	0.18(11)	52.07(7)	100.65
	py (2)	47.39(62)	0.08(2)	50.54(44)	98.01
	py (4)	47.59(76)	0.00(0)	52.2(50)	99.79
5H17	po (3)	62.72(127)	0.80(6)	35.78(33)	99.30
	po (2)	62.25(34)	0.83(15)	36.49(40)	99.57
	rhodium (2)	1.17(15)	99.33(45)	0.44(17)	100.94
	$Rh_{17}S_{15}$ (2)	3.47(9)	77.39(166)	19.45(40)	100.31
	~rhodium(2)	34.74(7)	66.19(186)	0.60(40)	101.53
9H1-300	po (2)	54.97(65)	8.88(43)	36.14(54)	99.99
	po (2)	55.24(81)	8.89(53)	36.28(33)	100.41
	alloy (2)	21.82(32)	78.32(63)	0.05(5)	100.19
9H2-300	po (3)	55.01(86)	5.45(64)	39.28(28)	99.74
	po (2)	53.67(5)	6.68(16)	39.17(41)	99.52
	new ~py (2)	42.20(41)	6.89(7)	50.97(108)	100.06
9H3-300	po (4)	55.56(2)	6.32(22)	35.59(17)	97.47
	po (2)	52.77(17)	9.63(21)	36.41(0)	98.81
	po (2)	49.37(35)	13.35(86)	36.23(17)	99.15
	po (2)	51.30(44)	11.48(2)	36.43(16)	99.21
9H13-300	po (3)	61.15(10)	0.85(28)	36.80(63)	98.80
	po (4)	61.37(40)	1.20(14)	36.52(29)	99.09
	alloy (2)	0.93(35)	97.72(14)	0.07(4)	98.72
	$Rh_{17}S_{15}$ (2)	4.84(40)	74.72(45)	21.26(7)	100.82
	po (3)	62.60(22)	0.14(2)	36.46(12)	99.20

Numbers in round brackets next to the name of the phase indicate number of point analyses made of that phase. Compositions are reported in wt%.

pyrrhotite (~8 at.% Rh, 52.2 at.% S) – $Rh_{17}S_{15}$ (about 7.5 at.% Fe) – melt, dominate the central portions of the phase system. They are bounded and separated by two-phase fields of appreciable width.

The solubility of Rh in pyrrhotite attains 25.7 at.%. This extraordinarily large compositional field of Rh-enriched pyrrhotite was delineated by a number of charges. On the S-rich side, the field is limited by a fairly constant value of 55.5–56.5 at.% S. On the S-poor side, its limits become progressively richer in S, from 50 at.% S for Rh-free troilite to 54 at.% S toward its Rh-rich end (*e.g.*, at about 23 at.% Rh). The most Rh-rich tip comprises S values of 55 ± 0.5 at.% S.

The extensive compositional field of pyrrhotite is bounded primarily by two-phase fields *po*–alloy, *po*–$Rh_{17}S_{15}$ (between 8 and 26 at.% Rh in *po*) and *po*–"RhS_3" (from 2.6 at.% to 16.3 at.% Rh in S-rich *po*). The three-phase assemblages *po* – $Rh_{17}S_{15}$ – Rh_3S_4 and

po – Rh_3S_4 – Rh_2S_3 involve the most Rh-rich compositions of pyrrhotite. The assemblage *po* – Rh_2S_3 (0.3 at.% Fe) – "RhS_3"(1 at.% Fe) involves S-rich *po* with 16.3 at.% Rh.

The solubility of Fe in $Rh_{17}S_{15}$ reaches about 7.5 at.%, and the width of the phase field with respect to the Rh:S ratio was found to be about 1–2 at.%. The solubility of Fe in Rh_3S_4 and Rh_2S_3 is below 0.5 at.%. The microprobe-established composition of "RhS_3" appears to be centered on $Rh_{2.75}S_{7.25}$ instead of ideal RhS_3 (*i.e.*, $Rh_{2.5}S_{7.5}$). Up to 4 at.% Fe may substitute for Rh in this phase.

Phase Relations at 500°C

Phase-equilibrium studies indicate three Fe–Rh alloys, five binary sulfides and a ternary compound in the condensed system at this temperature. The melt phase that is present at 900°C is absent at 500°C, leaving a large field of the three-phase assemblage *po* (0.5 at.% Rh, 51.3 at.% S) – $Rh_{17}S_{15}$ (5.5 at.% Fe) – alloy (48.5 ± 1.0 at.% Rh) in the central portion of the system (Fig. 2).

The ranges in solid solution of Fe–Rh alloys at 500°C are as follows: α(Fe,Rh) contains up to 9.5 at.% Rh; α_1(Rh,Fe) covers the range 33.5–52.2 at.%, whereas the Fe-rich boundary of γ(Rh,Fe) is highly uncertain owing to extremely low reactivity: the majority of measured compositions cluster at and below 2.5 at.% Fe, but up to 9.5 at.% Fe was measured in several instances. The first compositional gap is associated with *po* of composition $Fe_{50}Rh_{0.01}S_{50}$, whereas the other is associated with $Rh_{17}S_{15}$, which may contain up to 4.3 at.% Fe.

The solubility of Rh in the monosulfide increases markedly from zero in troilite to 2.8 at.% Rh as the sulfur content approaches 52.5 at.% S (Fig. 2). The latter composition is associated with the thiospinel $Fe(Fe_{0.08}Rh_{1.92})S_4$. This thiospinel may be associated with pyrite (<0.1 at.% Rh), $Rh_{17}S_{15}$ (4 at.% Fe) and Rh_2S_3 (~0.5 at.% Fe). "RhS_3", the exact composition of which was discussed above, and which contains ≤1 at.% Fe, is associated with pyrite (≤0.05 at.% Rh found) and Rh_2S_3 (~0.3 at.% Fe).

Discussion

Our data on the Fe–Rh join at a temperature of 900°C do not differ appreciably from the information compiled by metallurgists (Massalski *et al*. 1986). This trend was found to continue toward higher temperatures in our studies of the system Fe–Cu–Rh–Pt–S at 1000° and 1100°C (Table 2; data from Makovicky *et al*., in prep.).

Results at 500°C show a more restricted range of composition for α(Fe,Rh) than that predicted in

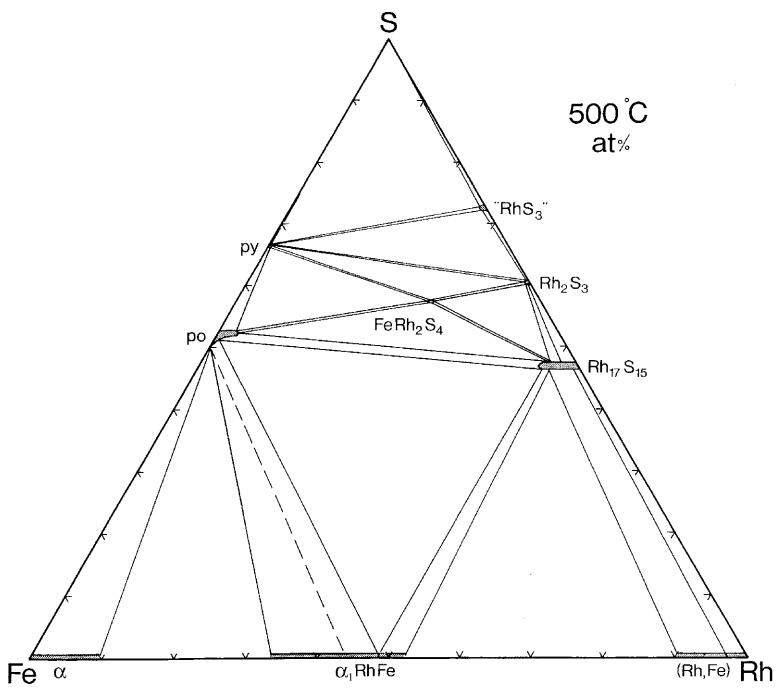

FIG. 2. The system Fe–Rh–S at 500°C. Width of field for solid phases (including alloys) is schematic except for pyrrhotite (*po*) and $Rh_{17}S_{15}$.

Massalski *et al*. (1986) and suggest an appreciable miscibility gap toward α_1(Fe,Rh) [this phase is denoted as α_1 in Kubaschewski (1982) but as α' in Massalski *et al*. (1986)]. The observed Fe-rich limit of the latter (equal to ~33.5 at.% Rh) is a direct continuation of that from higher temperatures. Therefore, we suggest that the continuous field α-Fe – α'(Fe,Rh) in the diagram of Massalski *et al*. (1986) is a metastable product of the treatment of metallurgical samples (annealing of the sample prepared at high temperatures), and that these phases are separated by a two-phase region at 500°C. The Rh-rich boundary of α'(Fe,Rh) agrees with that of Massalski *et al*.; our data on γ(Rh,Fe) are considered unreliable because of the lack of reactivity in low-S charges at 500°C. Still, the working hypothesis, based on our data, is that the γ(Rh,Fe) field at 500°C has a much more limited extent on the high-Fe side than the value of ~28 at.% Fe proposed tentatively by Massalski *et al*. (1986).

The solubility of Rh in pyrrhotite at 900°C agrees well with the data of Distler *et al*. (1988), who quoted 21 at.% Rh at 760°C. It was found essentially unchanged, ~27 at.% Rh, in the monosulfide solid-solution (*mss*) with ~56 at.% S and Ni/(Ni + Fe) in the range 0.45–0.55 in exploratory studies of the system Fe–Ni–Rh–S at 900°C (Makovicky *et al*. 1992). At 500°C, the solubility of Rh seems higher in *mss* [~6 at.% Rh for the most S-rich *mss* with Ni/(Ni + Fe) in the range 0.20–0.33] than in pure *po* (2.8 at.%).

Our studies corroborate the key role of pyrrhotite (*mss*) as a collector of Rh in ore deposits; indeed, the very high solubility of rhodium is quite exceptional among the platinum-group elements. In the case of Rh, the role of pyrrhotite should be comparable to or exceed that of pentlandite (Makovicky *et al*. 1986). Our results stress the key role of elevated fugacities of sulfur in this process. As is the case with the other PGE, Rh will concentrate in its alloys with Fe and not in pyrrhotite at low fugacities of sulfur.

Observations on natural material give a fairly complex picture of this problem. According to Distler *et al.* (1988) and Distler (1994), rhodium is the most important of the minor platinum-group elements in the copper–nickel ores of the Noril'sk region. It only rarely forms independent minerals, and is distributed between pyrrhotite and pentlandite, its contents being typically higher in pyrrhotite ores and lower in Cu-rich ores. Rh contents vary substantially in pyrrhotite; they are enriched in the ore rich in monoclinic (*i.e.*, S-rich) pyrrhotite. The investigations quoted reveal a nearly equal distribution between pyrrhotite and pentlandite, in agreement with the conclusions of Czamanske *et al.* (1992).

In the conditions of the Merensky Reef, with low proportions of monoclinic pyrrhotite, Rh concentrates heavily into pentlandite (Cabri 1992, Ballhaus & Ryan 1995); we can ascribe this pattern to a lower fugacity of sulfur in the Bushveld intrusion. Elsewhere, sulfarsenides (cobaltite, gersdorffite and hollingworthite) account for the bulk of Rh (*e.g.*, the Copper Cliff and Wellgreen deposits: Cabri 1992, Cabri *et al.* 1993), suggesting a potential redistribution of Rh exsolved from pyrrhotite, as suggested by Makovicky *et al.* (1986). Thus, in spite of the scarcity of data, measurements on natural pyrrhotite appear to confirm the predictions based on experiment results.

An occurrence of natural rhodian pyrrhotite is quoted by Cabri *et al.* (1996) from the placers of Chocó, Río Condoto, Colombia. The highest Rh content measured was 12.9 at.%, the lowest content 8.9 at.%. The same material was found to contain a porous rhodium–iron alloy in which the ratio of Rh (plus traces of Ir) to Fe is equal to one, and numerous grains of bowieite–kashinite solid solution (Rh_2S_3–Ir_2S_3), *i.e.*, these grains do not constitute a phase assemblage. Rhodian pyrrhotite with high rhodium content, $Fe_{0.79}Rh_{0.11}Cu_{0.04}Pt_{0.01}S_{1.00}$ occurs in form of blebs in isometric cavities in γ(Pt,Fe) alloys in the placers of the Pustaya River, Kamchatka, Russia (Tolstykh *et al.* 2000). Another quoted occurrence of rhodian pyrrhotite is the Ko River in the East Sayan Mountains, Russia (Tolstykh & Krivenko 1994).

Another Fe–Rh assemblage, encountered in the chromitites in the Fe-rich portions of a harzburgite block in the Krasnogorskiy massif (Koryak Mountains, Siberia) by Dmitrenko (1994), consists of a Fe–Rh alloy with a Fe:(Rh,Ir) ratio of about 1:1, hollingworthite, Rh-containing arsenides, rare $(Rh,Ir)_2S_3$ and rhodian pentlandite. A similar Fe–Rh alloy occurs with chromite in the Tropoja massif, Albania (Ohnenstetter *et al.* 1992). It is associated with Pt–Fe alloys, tulameenite, laurite, cooperite, hollingworthite, $(Ir,Rh)_2S_3$ and rhodian malanite. Rhodian pyrrhotite is not quoted.

The addition of Ni to the system enhances the formation of a sulfide melt; a melt with Ni/(Ni + Fe) ≈ 0.66 dissolves between 0 and ~45 at.% Rh at 900°C. As mentioned earlier, "RhS_3" has a very limited tolerance for Fe, even at 900°C. Addition of nickel to the system produces an extensive, possibly continuous, series "RhS_3" – NiS_2 with the Ni/(Ni + Fe) ratio in the solid solution rising progressively from 0.45 to 1.00 (Makovicky *et al.* 1992).

The references to thiospinel quoted in the introduction mention both $FeRh_2S_4$ and Fe_2RhS_4 (Raghavan 1988). However, in the system Fe–Rh–S, we found only

TABLE 2. COMPOSITION LIMITS FOR IRON–RHODIUM ALLOYS

T	γ (Fe,Rh)	α_1 (Fe,Rh)	γ (Rh,Fe)
1100°C	0 – 33	44.0 – 50.5	61.0 – 100
1000°C	0 – 34	41.5 – 52.0	63.5 – 100
900°C	~2 – 29.7	40.0 – 50.4	65.7 – 100

Compositions are quoted in at.%.

near-stoichiometric $FeRh_2S_4$ in association with *po* and pyrite. In contrast, addition of nickel to the system produces both $(Fe,Ni)Rh_2S_4$ [$0.10 < Ni/(Ni + Fe) < 0.20$] and $(Ni,Fe)_2RhS_4$ [$0.59 < Ni/(Ni + Fe) < 0.76$]. The former exhibits partial solid-solution toward the latter. However, $(Ni,Fe)_2RhS_4$ itself exhibits a range in solid solution that extends primarily in the direction of $FeNi_2S_4$ (Makovicky *et al.* 1992).

Acknowledgements

This paper is dedicated to our long-time friend and senior colleague, the doyen of the platinum-group studies, Dr. Louis J. Cabri. This research was supported by the EEC project No. BE–5793 and Danish Natural Science Research Council project No. 11–8878. The assistance of Mrs. Birthe Møller, Mrs. Maybritt Handest, Mrs. Camilla Sarantaris, Mr. John Fløng and Dr. S. Karup-Møller (Danish Technical University) as well as the valuable comments by Dr. L.J. Cabri and the editor, Prof. R.F. Martin, are gratefully acknowledged.

References

Ballhaus, C. & Ryan, C.G. (1995): Platinum-group elements in the Merensky Reef. 1. PGE in solid solution in base metal sulfides and the down-temperature equilibration history of Merensky ores. *Contrib. Mineral. Petrol.* **122**, 241-251.

Blasse, G. & Schipper, D.J. (1964): Sulphospinels containing rhodium. *J. Inorg. Nuclear Chem.* **26**(8), 1467-1468.

Bryukvin, V.A., Fishman, B.A., Reznichenko, V.A., Kukoyev, V.A. & Vasilyeva, N.A. (1990): Investigation of the Fe–Rh–S phase diagram in the Fe–Rh–Rh_2S_3–$FeS_{1.09}$ composition range. *Izv. Akad. Nauk SSSR, Metally* **1990**(2), 23-28 (in Russ.).

Cabri, L.J. (1992): The distribution of trace precious metals in minerals and mineral products. *Mineral. Mag.* **56**, 289-308.

_____, Harris, D.C. & Weiser, T.W. (1996): Mineralogy and distribution of platinum-group mineral (PGM) placer deposits of the world. *Explor. Mining Geol.* **5**, 73-167.

_____, Hulbert, L.J., Laflamme, J.H.G., Lastra, R., Sie, S.H., Ryan, C.G. & Campbell, J.L. (1993): Process mineralogy of samples from the Wellgreen Cu–Ni–Pt–Pd deposit, Yukon. *Explor. Mining Geol.* **2**, 105-119.

Czamanske, G.K., Kunilov, V.E., Zientek, M.L., Cabri, L.J., Likachev, A.P., Calk, L.C. & Oscarson, R.L. (1992): A proton-microprobe study of magmatic sulfide ores from the Noril'sk–Talnakh district, Siberia. *Can. Mineral.* **30**, 249-287.

Distler, V.V. (1994): Platinum mineralization of the Noril'sk deposits. *In* Proc. Sudbury–Noril'sk Symposium (P.C. Lightfoot & A.J. Naldrett, eds.). *Ontario Geol. Surv., Spec. Vol.* **5**, 243-260.

_____, Grokhovskaya, T.L., Evstigneyeva, T.L., Sluzhenikin, S.F., Filimonova, A.A. & Laputina, I.P. (1988): Distribution, mineral composition and zoning of copper–nickel ores. *In* Petrology of the Sulfide Magmatic Ore Formation (I.D. Ryabchikov, ed.). Nauka Publ. House, Moscow, Russia (in Russ.).

_____, Malevsky, A.Yu. & Laputina, I.P. (1977): Distribution of platinoids between pyrrhotite and pentlandite during the crystallization of sulfide melt. *Geochem. Int.* **14**(6), 30-40.

Dmitrenko, G.G. (1994): *Platinum-Group Minerals of Alpinotype Ultramafites*. Russ. Acad. Sci., Far East Branch, Magadan, Russia (in Russ.).

Harada, S. (1973): Some new sulfo-spinels containing iron-group transition metals. *Mater. Res. Bull.* **8**, 1361-1370.

Kubaschewski, O. (1982): *Iron – Binary Phase Diagrams*. Springer, New York, N.Y.

Makovicky, E., Rose-Hansen, J., Makovicky, M. & Rønsbo, J. (1992): The Fe- and Ni:Fe = 1:1 sections of the phase system Rh–Ni–Fe–S at 900° and 500°C. *Rapport til Statens Naturvidenskabelige Forskningsråd, Proj.* **11-8878**.

Makovicky, M., Makovicky, E. & Rose-Hansen, J. (1986): Experimental studies on the solubility and distribution of platinum group elements in base metal sulfides in platinum deposits. *In* Metallogeny of Basic and Ultrabasic Rocks (M.J. Gallagher, R.A. Ixer, C.R. Neary & H.M. Prichard, eds.). Institution of Mining and Metallurgy, London, U.K. (415-425).

Massalski, T.B., Murray, J.L., Bennett, L.H. & Baker, H. (1986): *Binary Alloy Phase Diagrams*. Vol. 1 and 2. American Society for Metals, Metals Park, Ohio.

Ohnenstetter, M., Vaughan, D., Makovicky, E., Rose-Hansen, J. & Ohnenstetter, D. (1998): New exploration method for platinum and rhodium deposits poor in base metal sulfides. Synthesis report. BRITE/EURAM *Project No.* **BE-5973**. BRGM, Orléans, France.

Raghavan, V. (1988): *Phase Diagrams of Ternary Iron Alloys*. **2**. *Ternary Systems Containing Iron and Sulphur*. The Indian Institute of Metals, Calcutta, India.

Sinyakova, Ye.F., Fedorova, Zh.N. & Kolonin, G.R. (1994): Behaviour of platinum, palladium and rhodium in the crystallization process of iron–nickel sulfide melts based on experimental data. *In* Geology and Origins of the Deposits of Platinum-Group Metals (N.P. Laverov & V.V. Distler, eds.). Nauka, Moscow, Russia (264-277; in Russ.).

Tolstykh, N.D. & Krivenko, A.P. (1994): On the composition of sulfides containing platinum-group elements. *Zap. Vses. Mineral. Obshchest.* **123**(2), 41-49 (in Russ.).

_____, Sidorov, E.G., Laajoki, K.V.O., Krivenko, A.P. & Podlipskiy, M. (2000): The association of platinum-group minerals in placers of the Pustaya River, Kamchatka, Russia. *Can. Mineral.* **38**, 1251-1264.

TRETYAKOV, YU.D., GORDEEV, I.V. & KESLER, YA.A. (1977): Investigation of some chalcogenides with spinel structure. *J. Solid State Chem.* **20**, 345-358.

Received August 20, 2000, revised manuscript accepted October 8, 2001.